Vibrational Analysis of Amino Acids and Short Peptides in Hydrated Media. VI. Amino Acids with Positively Charged Side Chains: L-Lysine and L-Arginine

Belén Hernández,[†] Fernando Pflüger,[†] Najoua Derbel,[‡] Joël De Coninck,[§] and Mahmoud Ghomi*,[†]

Groupe de Biophysique Moléculaire, UFR SMBH, Université Paris 13, 74 rue Marcel Cachin, 93017 Bobigny cedex, France, Laboratoire de Spectroscopie Atomique Moléculaire et Applications (LASMA), Département de Physique, Faculté des Sciences de Tunis, Campus Universitaire, 2092 EL MANAR II, Tunisia, and Centre de Recherche en Modélisation Moléculaire (CRMM), Université de Mons-Hainaut, Materia Nova, Parc Initialis, Avenue Copernic 1, B-7000 Mons, Belgium

Received: October 5, 2009; Revised Manuscript Received: November 4, 2009

In two recent reports of the same series (*J. Phys. Chem. B* **2007**, *111*, 1470−1477 and *J. Phys. Chem. B* **2009**, *113*, 3169−3178), we have described the geometrical and vibrational analysis of glycine and amino acids (AAs) with hydrophobic side chains through the joint use of optical spectroscopy and quantum mechanical calculations. Here, we report Raman scattering and Fourier-Transform Infrared (FT-IR) Attenuated Total Reflectance (ATR) spectra measured from the aqueous solutions (H_2O and D_2O) of L-lysine and L-arginine, i.e. two α-AAs with positively charged hydrophilic side chains. The discussion on the vibrational features of both AAs could be carried out thanks to the theoretical calculations performed by means of the Density Functional Theory (DFT) approach at the B3LYP/6-31++G* level. We have analyzed the influence of implicit (with a polarizable dielectric continuum) and explicit (by means of an H_2O cluster interacating with H-donor and H-acceptor sites of AAs) hydration models. In addition, through the calculated geometrical parameters and vibrational wavenumbers, a discussion was performed on the effect of the Cl^- anion interacting with the positively charged side chains of explicitely hydrated AAs.

I. Introduction

Lysine (K or Lys) belongs to essential and arginine (R or Arg) to conditionally essential groups of AAs. They cannot thus be synthesized by the organism and should be supplied by the daily diet.[1−3]

Both amino acids, together with histidine (H), form the group of positively charged amino acids (PCAAs). The extra positive charge of K and R arises from the nitrogen-containing chemical groups located at the ultimate position of their side chains, i.e., the protonated amino group $-NH_3^+$ (K) and the guanidinium group $[-NH-C-(NH_2)_2]^+$ (R) (Figure 1). In histidine, the protonation of the side chain ring is responsible for its cationic character.[4]

PCAAs participate in many important biological processes in living organisms. First of all, their role in protein/nucleic acid interactions, basically through the long-range order electrostatic attraction between the AA side chains and nucleic acid phosphate groups, should be emphasized. Indeed, DNA condensation into nucleosomes (building block of a chromatine) is made possible by the intermediate of five histone proteins:[5,6] H1 (K-rich), H2A, H2B (both moderately K-rich), H3, and H4 (both R-rich).[7] K, R, and also H, spaced by neutral hydrophobic AAs, form tetrapeptide repeats in the center of the KR-rich histone of calf thymus.[8] Different membrane proteins conform to a *positive-inside-rule*; i.e., PCAAs are located in their cytoplasmic domains. As a consequence, the topology of *E. coli* inner membrane proteins was found to depend on the number of K and R, flanking the apolar transmembrane segments.[9] Moreover, the presence and position of PCAAs in proteins are also pivotal in numerous important biological processes. For instance, it has been shown that these AAs (i) are located similarly in the toxins of different species such as sea anemone and scorpion, thus being essential in their interactions with their membrane receptor,[10] (ii) are fundamental in ligand binding and

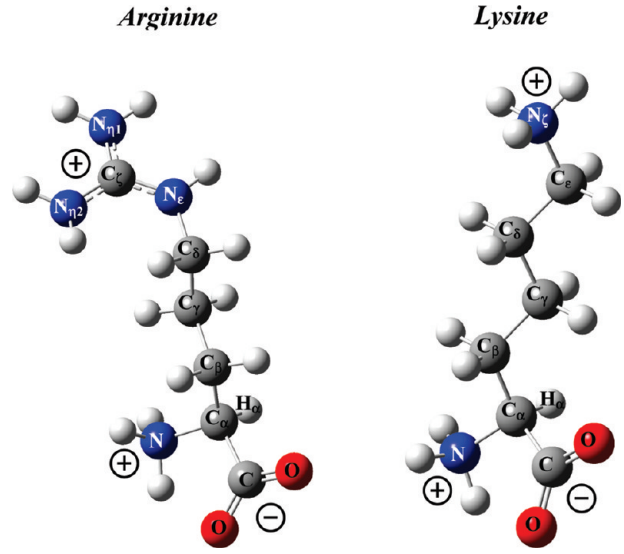

Figure 1. Amino acids with positively charged branched side chains: L-lysine (K) and L-arginine (R). Note that the extra positive charge of both amino acids arises from the nitrogen-containing chemical groups located at the ultimate position of their side chains, i.e., the protonated amino group $-NH_3^+$ and the guanidinium group $[-NH-C-(NH_2)_2]^+$ in K and R, respectively.

* To whom correspondence should be addressed. E-mail: mahmoud.ghomi@univ-paris13.fr.
† Université Paris 13.
‡ Faculté des Sciences de Tunis.
§ Université de Mons-Hainaut.

10.1021/jp909517r
Published on Web 12/21/2009

TABLE 1: Vibrational Modes of Lysine Observed in Aqueous Solutions (H_2O) and Their Assignments[a]

Raman	IR	calcd K/8H_2O/Cl^- (I)	assignments (PED %) (I)	calcd K/8H_2O/Cl^- (II)	assignments (PED %) (II)
1650 (w)		1777	NζH_3^+ asym bend (42); W6	1769	NζH_3^+ asym bend (51); W6; W8
	1636 (sh)	1763	NζH_3^+ asym bend (36); W8; W6	1753	NζH_3^+ asym bend (42); W6; W7; W8
1615 (w)		1751	NtH_3^+ asym bend (30)	1750	NtH_3^+ asym bend (37); W1
		1685	NtH_3^+ asym bend (28); H−O−H (W3) (26); W3	1685	NtH_3^+ asym bend (27); H−O−H (W6) (14); CtOO^- asym st (10)
1598 (w)	1599 (s)	1655	CtOO^- asym st (45); H−O−H (W3) (22)	1645	H−O−H (W6,W3) (31); CtOO^- asym st (31)
	1523 (s)	1616	NtH_3^+ sym bend (33); NtH_3^+ sym rock (31); W3	1619	NtH_3^+sym bend (32); NtH_3^+ sym rock (30); W3; W2
1470 (sh)	1473 (sh)	1535	Cε-bend (63); Cδ-bend (24)	1549	Cδ-bend (74); Cε-bend (15)
	1462 (sh)	1519	Cδ-bend (41); Cε-bend (34); Cγ-bend (22)	1528	Cε-bend (82); Cδ-bend (15)
1446 (s)		1511	Cβ-bend (93)	1516	Cγ-bend (80); Cβ-bend (11)
	1445 (sh)	1510	Cγ-bend (67); Cδ-bend (30)	1510	Cβ-bend (83); Cγ-bend (11)
1415 (s)		1448	Cδ-rock (22); Cε-rock (19); Cγ-rock (11); Nt-Cα-Hα	1468	Cδ-rock (64); Cε-rock (13); Cγ-rock (10)
	1413 (s)	1442	Cε-rock (25); CtOO^- sym st (13); Cδ-rock (12); Nt-Cα-Hα (10)	1437	Nt-Cα-Hα (24); CtOO^- sym st (17); Cβ-rock (15)
		1420	Cγ-rock (39); Cε-rock (26)	1410	Cε-rock (36); Cδ-twist (17); Cγ-rock (9)
		1410	Cβ-Cα-Hα (27); Nt-Cα-Hα (13); Cβ-twist (11); CtOO^- sym st (10)	1406	Cδ-twist (17); Cε-rock (16); -CβCα-Hα (11); CtOO^- sym st (10); Cγ-rock (10)
		1396	Cβ-rock (33); Nt-Cα-Hα (19); Cγ-wag (14)	1403	Cδ-twist (37); Hα−Cα−Cβ (11)
		1380	Cε-twist (41); NζH_3^+ asym rock (22)	1389	Cβ-rock (45); Nt-Cα-Hα (15)
1353 (s)	1352 (s)	1367	Cδ-twist (49); Cγ-wag (9); Cε-twist (9)	1367	Cε-twist (40); NζH_3^+ asym rock (17); W6
1328 (s)	1329 (s)	1360	CtOO^- sym st (28); Cβ-twist (18)	1364	CtOO^- sym st (15); Cγ-rock (15); Cβ-twist (14); Cδ-rock (10)
	1315 (sh)	1347	Cδ-rock (27); Cγ-rock (18); Cδ-twist (10)	1350	CtOO^- sym st (19); Cγ-rock (16); Ct-Cα-Hα (12)
		1318	Cγ-wag (38); Cδ-wag (9)	1307	Cγ-wag (46); Cδ-wag (9)
1293 (sh)	1292 (w)	1263	Cβ-twist (27); Ct-Cα-Hα (10); NζH_3^+ asym rock (8)	1252	Cβ-twist (33); Hα-Cα-Ct (11); Cγ-rock (9)
1234 (w)		1241	Cγ-twist (13); NtH_3^+ asym rock (12); Cβ-Cα-Hα (10); Cδ-wag (10)	1238	NtH_3^+ asym rock (15); Cγ-twist (12); Cδ-wag (11)
1183 (m)	1181 (w)	1214	NζH_3^+ asym rock (21); Cε-rock (14)	1194	NζH_3^+ asym rock (25); Cε-rock (14)
1143 (m)	1143 (m)	1179	NtH_3^+ asym rock (39); Ct Cα-Hα (18)	1177	NtH_3^+ asym rock (41); Ct-Cα-Hα (15)
1076 (sh)		1095	Cγ-Cδ (36); Cβ-Cγ (26)	1099	Cγ-Cδ (44); Cβ-Cγ (12)
1063 (m)		1078	Cδ-Cε (13); Cε-Nζ (12); Cδ-wag (11)	1067	Cγ-twist (11); Cδ-wag (11); W6; Cδ-Cε (10); Cε-twist (9)
1033 (sh)		1071	Cε-Nζ (43); Cδ-Cε (19)	1052	Cδ-Cε (30); Cε-Nζ (15)
1012 (m)		1055	Cβ-Cγ (17); Cβ-wag (12); Cγ-scissor (12)	1042	Cβ-Cγ (27); Cα-Cβ (13); Cε-Nζ (10)
	1007 (m)	1012	Cα-Cβ (22); Cγ-Cδ (21); Cε-Nζ (14)	1007	Cε-Nζ (36); Cγ-Cδ (14); Cα-Cβ (14); Nt-Cα (12)
961 (w)		994	Nt-Cα (29); Cδ-Cε (12)	986	Nt-Cα (23); W4; W2
919 (sh)		957	Cε-wag (11); Cα-Cβ (9)	950	Cε-wag (16)
903 (m)		914	Cγ-Cδ (10); Cβ-wag (10); Cβ-Cγ (9); Nt-Cα (9); Cα-Ct (9)	913	Cα-Ct (12); Cβ-Cγ (12); Cβ-wag (12)
847 (s)		863	Cγ-twist (13); Cε-wag (13); Cβ-wag (10)	859	Cγ-twist (26); Cε-wag (23)
819 (sh)		831	O−Ct−O (13)	845	O−Ct−O (19); Cβ-wag (14); CαCtOO^- sym bend (9)
745 (w)		750	Cδ-wag (18); Cγ-twist (14); Cl^-; W7	760	Cδ-wag (28); Cγ-twist (17); τ(Cγ-Cδ) (9)

[a] s, intense; m, medium; w, weak; sh, shoulder. Raman: Raman spectra recorded in H_2O buffers (Figure 2). IR: FT-IR ATR spectra recorded in H_2O (Figure 2). Calcd: Calculated wavenumbers obtained at the DFT/B3LYP/6-31++G* the level. K/8H_2O/Cl^-: Neutral system formed by lysine surrounded by 8 water molecules and a Cl^- anion (Figure 6). (I) and (II) correspond to the two optimized clusters shown in Figure 6. Assignments are based on the Potential Energy Distribution (PED). Only major contributions (PED ≥ 9%) are reported. The angular bending modes of the tetrahedrons located along the K side chain are referred to as bending (-bend), wagging (-wag), twisting (-twist), rocking (-rock), and scissoring (-scissor). τ designates a torsional internal coordinate. For atom numbering, see Figure 1. Water molecules are numbered from W1 to W8 (Figure 6).

signal transduction,[11] (iii) are responsible for the rectification of inward−outward currents through the ionic channels, by their presence on the wall of the cytoplasmic pore,[12] and (iv) are essential in enzymatic reactions appearing through digestive system. The action of trypsin that cleaves peptide chains at the carboxyl side of the K (or R) is to be noted.[13]

Beyond all these characteristics, since the discovery of the translocation of the third helix of the homeodomain of Antennapedia through the biological membranes,[14] peptides are considered as important molecular tools for drug delivery into cells.[15,16] In this framework, the capability of the amphipathic peptides, formed by an adequate combination of hydrophilic (basically K and R) and hydrophobic amino acids, was proved through the delivery of therapeutic DNA (antisense oligonucleoties, plasmids, ...).[15−18]

It is a matter of fact that vibrational spectroscopy (Raman scattering and IR absorption) can be considered as rapid and efficient tools to elucidating the secondary structure of peptides and proteins, as well as their interactions with other molecules (nucleic acids, proteins, membranes, drugs, ...). In this framework, it is a fundamental task to achieve a good knowledge of the vibrational features of the peptide building blocks. We have recently reported and discussed in the manuscripts I and IV of this series[19,20] the vibrational data from glycine and the amino acids with branched hydrophobic side chains (alanine, valine, isoleucine, leucine). In the present manuscript, our aim is to extend our analysis to lysine and arginine. Obviously, the present investigation uses as background all the experimental and theoretical works reported previously, among which should be mentioned: (i) Raman spectra obtained from L-arginine·$HCl·H_2O$ single crystal as a function of temperature,[21] (ii) FT-Raman and ATR FT-IR spectra of L-arginine·$HNO_3·0.5H_2O$,[22] (iii) Raman spectra obtained from the solutions of L-lysine and its C-deuterated derivative,[23] (iv) FT-IR spectra of both AAs recorded in aqueous solutions,[24] and (v) ab initio calculations on the stability neutral and zwitterionic forms of isolated L-arginine.[25] Here we report Raman and FT-IR spectra of both AAs, recorded in H_2O and D_2O along with their interpretation by means of ab initio calculations.

II. Materials and Methods

Experimental. Monohydrochloride salts of K and R were purchased as lyophilized powder samples from Sigma-Aldrich. Water was taken from a Millipore filtration system. Heavy water (100% purity) was provided by Euriso-top (Saclay, France). Powder samples were dissolved in H_2O (or D_2O) to obtain aqueous solutions of each amino acid at 50 mM and 100 mM molecular concentrations for Raman and FT-IR measurements, respectively. To avoid D_2O/H_2O exchange, deuterated samples were prepared under a dry air atmosphere. For recording Raman spectra, 30 μL of solution placed in suprasil quartz cells (5 mm path length) was excited by the 488 nm line emitted by an Ar^+ laser (Spectra Physics). Scattered light at a right angle was analyzed on a Jobin-Yvon T64000 spectrograph in a single spectrograph configuration with a 1200 grooves/mm holographic grating and a holographic notch filter. A liquid nitrogen cooled CCD detection system (Spectrum One, Jobin-Yvon) based on a Tektronix CCD chip of 2000 × 800 pixels was used to collect Stokes Raman data with an accumulation time of 40 min, using an effective spectral slit width set to ca. 5 cm^{-1}. FT-IR spectra were recorded on a Perkin-Elmer 2000 spectrophotometer under continuous dry air purge and equipped with a ZnSe crystal ATR accessory. To record each spectrum, 18 μL of a sample solution was deposed in drops on the ATR crystal and spread to cover the whole surface. The incident infrared beam meeting the ATR crystal surface under an effective angle of 45°, followed then 12 reflections from the entrance to the exit points. Each infrared spectrum corresponds to 20 scans and was collected with 1 cm^{-1} spectral resolution and a medium Norton Beer apodization function. Postprocessing of Raman spectra, including subtraction of buffer contribution, baseline correction, and smoothing, was performed by means of GRAMS/32 software (Galactic Industries). ATR data treatment was carried out by the Perkin-Elmer Spectrum program. The final presentation of vibrational spectra has been performed by means of the SIGMAPLOT package.

Theoretical. The density functional theory (DFT) approach[26] by means of B3LYP functionals, i.e., Becke's three parameter (B3) exchange functional[27] with the Lee−Yang−Parr (LYP) nonlocal correlation functional,[28] was used to estimate geometrical and harmonic modes of cationic AAs. Standard split valence, double-ζ Gaussian atomic basis sets containing diffuse functions on heavy and hydrogen atoms, as implemented in the GAUSSIAN03 pakage,[29] and referred to as 6-31++G*, were employed. As in our previous calculations on amino acids,[19,20] we have attempted to consider the effect of hydration on the vibrational features. Two hydration models were considered in this work based on: (i) an implicit hydration by means of a polarizable dielectric continuum model (COSMO),[30,31] basically capable of mimicking an environment such as that created by bulk water around a molecule and (ii) an explicit hydration by the intermediate of n water molecules surrounding the solvated molecule, where n is minimally but significantly selected to reproduce the H-bond interactions with all the acceptor and donor sites of both AAs, such as NH_3^+, NH_2, NH, and COO^- (Figure 1). Recently, through a systematic investigation on leucine,[20] an AA with a large size hydrophobic side chain, we have shown that a cluster of $5H_2O$ can hydrate accurately its backbone by maintaining its zwitterionic character. On the basis of this result and also on those derived from other AAs with hydrophobic side chains,[20] we have derived the conclusion that for a reasonable and accurate hydration we should use as many water molecules as there are potential H-acceptor and H-donor sites in a molecule. The side chains of lysine and arginine possess 3 and 5 NH bonds, respectively. Consequently, quantum mechanical calculations were performed on the clusters containing 8 or 10 water molecules, hereafter referred to as K/$8H_2O$ and R/$10H_2O$. Note that these two clusters, as well as that formed by lysine embedded in a dielectric continuum, referred to as K/dielec, are positively charged; i.e., each of them contains one extra positive charge. As the samples used for Raman and FT-IR experiments contain Cl^- counterions (see above, Experimental), neutralizing the positive charge of their side chains, we have also performed further calculations which have allowed us to analyze the counterion effect in the neutral clusters K/$8H_2O$/Cl^- and R/$10H_2O$/Cl^- on both geometrical and vibrational data of hydrated AAs. The geometry of the above-mentioned systems was first fully optimized, before procceeding to harmonic vibrational calculations. The absence of imaginary frequency proved the assignment of an optimized geometry to a local minimum in the molecular energy landscape. Values of the electronic (E_e) and vibrational energies ($E_v = 1/2\ \Sigma\ h\nu$, where h is the Plank constant and ν the frequency of a

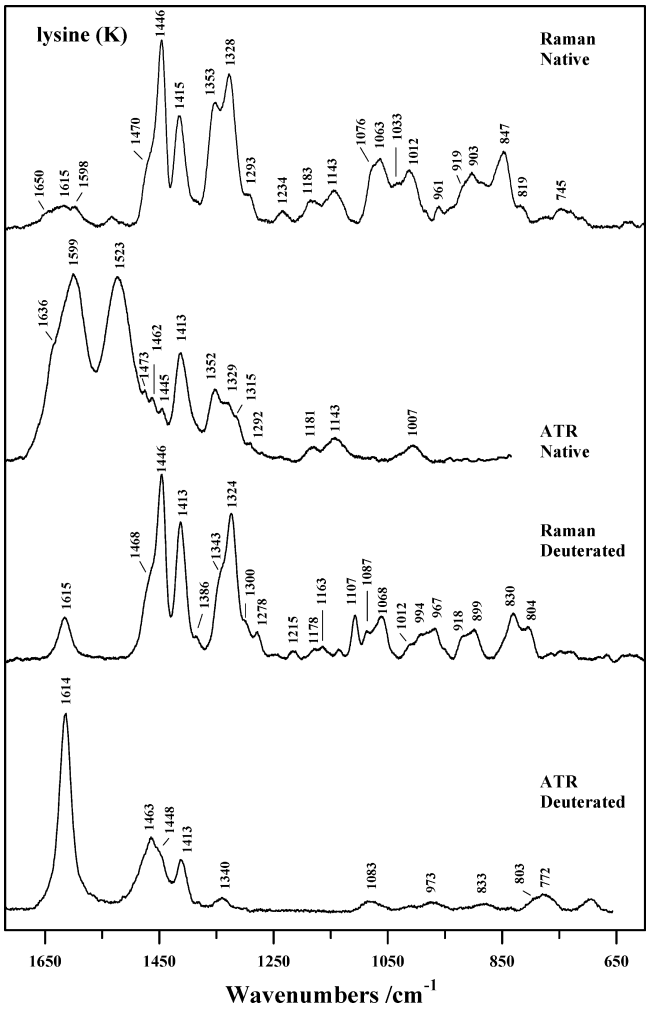

Figure 2. Vibrational spectra of lysine (K) observed in aqueous solutions. From top to bottom: Raman spectrum recorded in H_2O buffer ($\lambda_L = 488$ nm), FT-IR ATR spectrum recorded in H_2O, Raman spectrum recorded in D_2O buffer ($\lambda_L = 488$ nm), FT-IR ATR spectrum recorded in D_2O. The intensity of each observed spectrum was normalized to the most intense peak to facilitate their comparison.

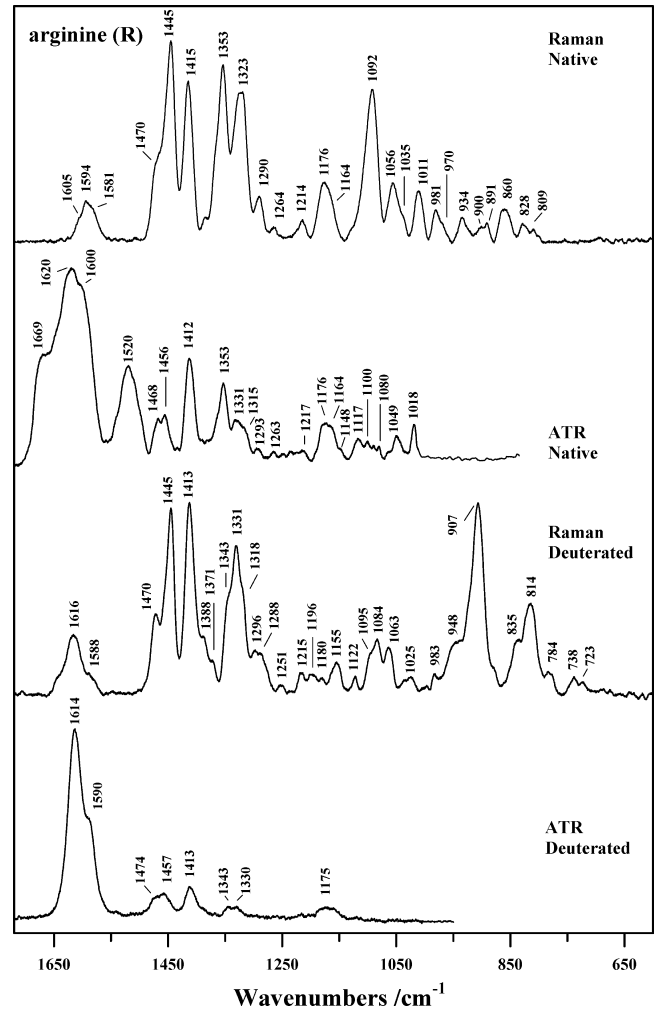

Figure 3. Vibrational spectra of arginine (R) observed in aqueous solutions. From top to bottom: Raman spectrum recorded in H_2O buffer ($\lambda_L = 488$ nm), FT-IR ATR spectrum recorded in H_2O, Raman spectrum recorded in D_2O buffer ($\lambda_L = 488$ nm), FT-IR ATR spectrum recorded in D_2O. The intensity of each observed spectrum was normalized to the most intense peak to facilitate their comparison.

vibrational mode) were estimated from the quantum mechanical calculations carried out on different models of solvated AAs.

Harmonic force constants, output from Gaussian, were post-treated by a homemade program (BORNS), allowing us to remove redundancies among vibrational coordinates and to assign wavenumbers on the basis of the PED (Potential Energy Distribution) matrix elements as expressed in terms of a combination of local symmetry and internal coordinates. Local symmetry coordinates were preferentially used to achieve a better analysis of the vibrational modes arising from the CH_2, NH_2, NH_3^+, and COO^- groups involved in the chemical constitution of the studied AAs (see also refs 19, 20, and 32 for more details). No scaling factor was used to improve the agreement between calculated and observed wavenumbers. In fact, the report of raw calculated wavenumbers leads to a better estimation of the inaccuracies related to the theoretical level, basis sets, as well as to the neglect of anharmonic effects.

III. Results

Observed vibrational spectra obtained from the aqueous samples of lysine and arginine are displayed in Figures 2 and 3, respectively. In each figure, Raman and FT-IR spectra corresponding to the AAs dissolved in H_2O (native species) and D_2O (labile-hydrogen deuterated species) are presented. To facilitate the comparison between these spectra, each of them was normalized to its most intense peak. The wavenumbers of the main observed bands, together with their relative intensities, are also reported in Tables 1 and 2 for lysine and Tables 3 and 4 for arginine.

From the theoretical point of view, the streoviews of the optimized geometries of lysine and arginine in hydrated media (dielectrique continuum for K and explicit hydration for both K and R) are shown in Figures 4−6. Electronic and vibrational energies obtained from different molecular systems are indicated in Table 5. Tables S1 and S2, reporting the geometrical parameters of K and R in different environments, are provided as Supporting Information. In Table 6, the influence of implicit and explicit hydrations, as predicted by theoretical calculations, on a selection of characteristic vibrational modes, is indicated. The comparison between the observed and theoretical wavenumbers corresponding to native and deuterated species of both AAs, together with their calculated assignments, is performed in Tables 1−4.

TABLE 2: Vibrational Modes of Lysine Observed in Aqueous Solutions (D_2O) and Their Assignments[a]

Raman	IR	calcd K/8D_2O/Cl^- (I)	assignments (PED %)	calcd K/8D_2O/Cl^- (II)	assignments (PED %)
1615 (m)	1614 (s)	1688	$CtOO^-$ asym st (80); $C\alpha CtOO^-$ asym bend (10)	1683	$CtOO^-$ asym st (82); $C\alpha CtOO^-$ asym bend (10)
1468 (sh)	1463 (m)	1535	Cε-bend (62); Cδ-bend (25)	1550	Cδ-bend (76); Cε-bend (14)
	1448 (sh)	1519	Cδ-bend (41); Cε-bend (35); Cγ-bend (20)	1528	Cε-bend (83); Cδ-bend (15)
1446 (s)		1512	Cβ-bend (94)	1516	Cγ-bend (79); Cβ-bend (12)
1413 (s)	1413 (m)	1510	Cγ-bend (68); Cδ-bend (29)	1511	Cβ-bend (82); Cγ-bend (12)
		1445	Cδ-rock (37); Cε-rock (21); Cγ-rock (17)	1469	Cδ-rock (66); Cε-rock (12); Cγ-rock (10)
1386 (w)		1435	$CtOO^-$ sym st (25); Cβ-rock (18)	1428	Cβ-rock (26); $CtOO^-$ sym st (25); Nt-Cα-Hα (13)
		1412	Cγ-rock (31); Cε-rock (27); Cβ-twist (13)	1406	Cδ-twist (59)
		1407	Cβ−Cα−Hα (18); Cβ-rock (13); Cε-rock (12); $CtOO^-$ sym st (11); Cγ-rock (10)	1402	Cβ−Cα−Hα (16); Cβ-twist (15); Cδ-twist (13); Cβ-rock (10)
1343 (sh)		1375	Nt-Cα-Hα (27); Cγ-wag (26); Cβ-rock (13); Cβ-Cα-Hα (12); Cδ-twist (11)	1396	Cε-rock (40); Cγ-rock (28)
	1340 (w)	1364	Cδ-twist (45); Cε-twist (17); Cβ-rock (9);	1369	Ct-Cα-Hα (35); Cβ-rock (26); Cγ-wag (12)
1324 (s)		1354	Cβ-twist (23); $CtOO^-$ sym st (22); Ct-Cα-Hα (9)	1358	Cβ-twist (20); Cε-rock (19); $CtOO^-$ sym st (17); Cδ-rock (11)
1300 (sh)		1334	Cε-twist (40); Cγ-wag (12)	1340	Ct-Cα-Hα (16); Cγ-rock (16); Cδ-rock (10); $CtOO^-$ sym st (9); Cε-rock (9)
		1330	Cδ-rock (30); Cγ-rock (13); Cε-rock (10)	1320	Cε-twist (51); Cγ-wag (13); W6
1278 (w)		1299	NζD_3^+ sym bend (22); NζD_3^+ sym rock (18); W6; W7	1285	Cγ-wag (16); NζD_3^+ sym bend (10); W6
		1282	Cγ-wag (14); Cε-twist (9)	1274	NζD_3^+ sym bend (9); Cγ-wag (9); W6
		1271	NζD_3^+ asym bend (37); W6; W8	1272	NζD_3^+ asym bend (47); W6; W8
1215 (w)		1250	NζD_3^+ asym bend (21)	1240	NζD_3^+ asym bend (21); W6; W7
		1230	Cβ-twist (17); (D−O−D) (W3) (14)	1228	Cβ-twist (11)
1178 (w)		1210	NtD_3^+ asym bend (31); W3	1209	NtD_3^+ asym bend (35); W3
1163 (w)		1177	Cγ-twist (15); Cδ-wag (14); Cα-Cβ (13); Cε-wag (11)	1173	Cγ-twist (14); Cα-Cβ (13); Cδ-wag (13); Cε-wag (11)
1107 (m)		1114	Cδ-Cε (23); Cε-scissor (10); Cγ-scissor (9); Cγ-Cδ (9)	1110	Cδ-Cε (18); Cγ-Cδ (12); Cγ-scissor (10); Cε-scissor (10)
1087 (sh)	1083 (w)	1094	Cβ-Cγ (30); Cγ-Cδ (22); Cα-Cβ (15)	1097	Cγ-Cδ (33); Cδ-Cε (22); Cβ-Cγ (15); Cα-Cβ (9)
1068 (m)		1067	Cδ-Cε (21); Cγ-Cδ (12); Cα-Cβ (12);	1065	Cα-Cβ (20); Cδ-Cε (16)
1012 (sh)		1038	Cε-Nζ (29); Cβ-Cγ (15); Cδ-Cε (9)	1025	Cβ-Cγ (21); Cε-Nζ (13); W6
994 (sh)		1012	Cε-Nζ (21)	1001	Cε-Nζ (22)
	973 (w)	996	Nt-Cα (32); Nt-Cα-Ct (11)	994	Nt-Cα (30); Nt-Cα-Ct (9)
967 (m)		967	Cγ-Cδ (22); Cε-Nζ (14); Cβ-Cγ (13); NtD_3^+ asym rock (12)	964	Cε-Nζ (30); Cγ-Cδ (15); Cβ-Cγ (13)
918 (sh)		917	Cγ-twist (19); NζD_3^+ asym rock (17)	917	Cγ-twist (23); NtD_3^+ asym rock (11); NζD_3^+ asym rock (9); W6
899 (m)		887	NζD_3^+ asym rock(15); Cβ-wag (13)	879	Cβ-wag (16); NζD_3^+ asym rock (13); Nt-Cα (11); W6
830 (m)	833 (w)	848	NζD_3^+ asym rock (18); Cδ-Cε (9)	839	NtD_3^+ sym rock (20); OCtO (18); C$\alpha CtOO^-$ sym bend (9)
		840	NζD_3^+ asym rock (17); Nt-Cα (13); OCtO (10)	829	NζD_3^+ sym rock (25)
		833	Cε-wag (12); NζD_3^+ asym rock (12)	824	NζD_3^+ sym rock (12); W6
804 (sh)	803 (sh)	804	Cε-wag (15); Cα-Cβ (10)	802	NζD_3^+ asym rock(12); Cε-wag (10)
	772 (w)	769	Cβ-wag (10); Nt-Cα-Ct (9); W4; W5	751	Cδ-wag (26); Cγ-twist (16); τ(Cγ-Cδ) (11)

[a] s, intense; m, medium; w, weak; sh, shoulder. Raman: Raman spectra recorded in H_2O buffers (Figure 2). IR: FT-IR ATR spectra recorded in H_2O (Figure 2). Calcd: Calculated wavenumbers obtained at the DFT/B3LYP/6-31++G* level. See also Figure 6 for optimized geometries. Assignments based on the Potential Energy Distribution (PED). Only major contributions (PED ≥ 9%) are reported. The angular bending modes of the tetrahedrons located along the K side chain are referred to as bending (-bend), wagging (-wag), twisting (-twist), rocking (-rock), and scissoring (-scissor). τ designates a torsional internal coordinate. For atom numbering, see Figure 1. Water molecules are numbered from W1 to W8 (Figure 6).

TABLE 3: Vibrational Modes of Arginine Observed in Aqueous Solutions (H_2O) and Their Assignments[a]

Raman	IR	calcd R/10H_2O	assignments (PED %)	calcd R/10H_2O/Cl^-	assignments (PED %)
	1669 (sh)	1770	NtH_3^+ asym bend (40); H−O−H (W2) (14)	1766	NtH_3^+ asym bend (36); NtH_3^+ asym bend (19); W2(H1−O−H2) (10)
		1762	NtH_3^+ asym bend (56)	1763	NtH_3^+ asym bend (25); NtH_3^+ asym bend (19); COO^- asym st (11)
	1620 (s)	1756	Nη2-H_2 bend (39); CζNη2H_2 sym bend (19)	1757	Nη1-H_2 (36); CζNη1H_2 sym bend (11); Nη1-Cζ - Nη2 asym st (9)
1605 (sh)	1600 (s)	1733	Nη1-H_2 bend (42); Nη1-Cζ-Nη2 asym st (19); CζNη2H_2 sym bend (17)	1681	Nη2-H_2 (41); CζNη2H_2 sym bend (15)
1594 (m)		1677	Nε-Cζ (17); H−O−H (W8) (13)		
1581 (sh)		1654	$CtOO^-$ asym st (42); H−O−H (W4, W3) (41)	1662	$CtOO^-$ asym st (40); H−O−H (W3, W4) (40)
	1520 (s)	1639	NtH_3^+ sym bend (38); NtH_3^+ sym rock (35)	1657	Nε-Cζ (20); CζNη2H_2 asym bend (11); Nη1-Cζ- Nη2 asym st (10)
		1614	Nε-Cζ (19); Nη1-Cζ- Nη2 asym st (16)	1635	NtH_3^+ sym bend (38); NtH_3^+ sym rock (35)
1470 (sh)	1468 (m)	1549	Cδ-bend (72); Cγ-bend (11)	1549	Cδ-bend (80)
		1531	Cγ-bend (49); Cβ-bend (29); Cδ-bend (16)	1530	Cγ-bend (50); Cβ-bend (34); Cδ-bend (11)
	1456 (m)	1521	Cβ-bend (60); Cγ-bend (32)	1519	Cβ-bend (58); Cγ-bend (38)
1445 (s)		1511	Nη1-Cζ-Nη2 asym st (24); Cδ-Nε-Hε (22); Cζ-Nε-Hε (13); W6	1499	Nη1-Cζ-Nη2 asym st (31); Cδ-Nε-Hε (12); W6
1415 (s)		1447	Cβ-rock (25); Cγ-wag (21); $CtOO^-$ sym st (12); Nt-Cα-Hα (9)	1449	Cγ-wag (41); Cβ-rock (20); Cδ-rock (14)
	1412 (s)	1431	Cγ-wag (25); Cδ-rock (20); Nt-Cα-Hα (16)	1427	Nt-Cα-Hα (22); Cδ-rock (14); $CtOO^-$ sym st (13)
1353 (s)	1353 (s)	1399	$CtOO^-$ sym st (25); Nt-Cα-Hα (25); Cβ-Cα-Hα (17)	1393	Nt-Cα-Hα (25); $CtOO^-$ sym st (20); Cβ-Cα-Hα (19)
	1331 (m)	1392	Cβ-rock (29); Cδ-rock (24)	1389	Cβ-rock (26); Cδ-rock (26)
1323 (s)	1315 (sh)	1371	Cβ-twist (23); $CtOO^-$ sym st (17); Cγ-rock (17); Cβ-Cα-Hα (10)	1370	Cγ-rock (28); Cβ-twist (24); $CtOO^-$ sym st (16)
1290 (m)	1293 (w)	1354	Cγ-rock (46); Cδ-twist (16)	1354	Cγ-rock (39); $CtOO^-$ sym st (13); Cδ-twist (10); Ct-Cα-Hα (9)
		1321	Cγ-wag (25); Cβ-rock (20); Cδ-twist (11)	1321	Cγ-wag (30); Cβ-rock (28); Cδ-rock (11)
1264 (w)	1263 (w)	1314	Cδ-twist (32); Cγ-wag (9); Cβ-twist (9)	1308	Cδ-twist (44); Cβ-twist (14); Cγ-twist (10)
1214 (m)	1217 (w)	1245	NtH_3^+ asym rock (17); Cβ-twist (12); Cδ-twist (10)	1249	Cδ-Nε (22); CζNη1H_2 asym bend (16); Nε-Cζ (15); CζNη2H_2 asym bend (15)
1176 (m)	1176 (m)	1220	CζNη2H_2 asym bend (30); Cδ-Nε (17); Nε-Cζ (14); W9	1241	NtH_3^+ asym rock (16); Cβ-twist (12)
1164 (sh)	1164 (sh)	1209	NtH_3^+ asym rock (20); Ct-Cα-Hα (17); Cβ-Cα-Hα (11); Cδ-wag (9)	1207	Cδ-wag (18); Cβ-Cα-Hα (12); NtH_3^+ asym rock (9)
	1117 (w)	1199	NtH_3^+ asym rock (29); Ct-Cα-Hα (11)	1186	NtH_3^+ asym rock (35); Ct-Cα-Hα (21)
1092 (s)	1100 (w)	1137	CζNη1H_2 asym bend (62)	1177	CζNη1H_2 asym bend (32); CζNη2H_2 asym bend (16); Nη1-Cζ - Nη2 asym st (11); Cl^-
	1080 (w)	1132	Cδ-Nε (29); Nη1-Cζ-Nη2 sym st (12)	1137	Cδ-Nε (28); Nη1-Cζ - Nη2 sym st (18); CζNη2H_2 asym bend (14)
1056 (m)		1122	Cγ-twist (11); Nη1-Cζ-Nη2 sym st (9)	1119	Cγ-twist (11); Cβ-wag (10); Cβ-twist (9); Ct-Cα-Cβ (9); Cδ-wag (9)
1035 (sh)	1049 (m)	1081	Cγ-Cδ (46)	1082	Cγ-Cδ (41)
1011 (m)	1018 (s)	1068	Cβ-Cγ (55)	1076	Cβ-Cγ (55); Cγ-Cδ (10)
981 (m)		1029	Cα-Cβ (31); Nt-Cα (23)	1026	Cα-Cβ (35); Nt-Cα (18)
970 (sh)		998	Nt-Cα (29); Cα-Cβ (15); Cα-Ct (13)	997	Nt-Cα(23); Cα-Ct (12); Cα-Cβ (10)
934 (w)		980	Nη1-Cζ-Nη2 sym st (19); Cδ-Nε (14); Cβ-Cγ (14); Nε-Cζ (13)	981	Nt-Cα (13); Cβ-Cγ (13); Nη1-Cζ-Nη2 sym st (13); Cγ-Cδ (11); Cδ-Nε (10)
900 (sh)		919	Cδ-wag (20); Cβ-wag (17)	911	Cδ-wag (13); W6
891 (w)				870	OCtO (12); W4
860 (m)		829	τ(Cζ -Nη2) (25); W7		
828 (w)				801	ω(Nη1-H_2) (20); W8; W10
809 (w)		779	Cγ-twist (23)	780	Cγ-twist (22); Cβ-Cα-Ct (14); τ(Cγ-Cδ) (11); Cδ-wag (9); W2; W4

[a] s, intense; m, medium; w, weak; sh, shoulder. Raman: Raman spectra recorded in H_2O buffers (Figure 3). IR: FT-IR ATR spectra recorded in H_2O (Figure 3). CalcD: Calculated wavenumbers obtained at the DFT/B3LYP/6-31++G* level. R/10H_2O: Positively charged cluster formed by arginine surrounded by 10 water molecules. See Figure 5 for optimized geometry and Table S2 (Supporting Information) for geometrical parameters. R/10H_2O/Cl^-: Neutral cluster formed by arginine surrounded by 10 water molecules and a Cl^- anion. See Figure 5 for optimized geometry and Table S2 (Supporting Information) for geometrical parameters. Assignments based on the Potential Energy Distribution (PED). Only major contributions (PED ≥ 9%) are reported. ω and τ designate an out-of-plane bending and a torsional internal coordinate, respectively. For atom numbering see Figure 1. Water molecules are numbered from W1 to W10 (Figure 5).

TABLE 4: Vibrational Modes of Arginine Observed in Aqueous Solutions (D_2O) and Their Assignments[a]

Raman	IR	calcd R/10D_2O	assignments (PED %)	calcd R/10D_2O/Cl^-	assignments (PED %)
1616 (s)	1614 (s)	1689	$CtOO^-$ asym st (86)	1694	$CtOO^-$ asym st (84)
1588 (sh)	1590 (sh)	1652	Nη1-Cζ-Nη2 asym st (36); Nε-Cζ (23); Nη1-Cζ-Nη2 sym st (12)	1652	Nε-Cζ (50); Nη1-Cζ- Nη2 sym st (18); Nη1-Cζ- Nη2 (12)
		1600	Nη1-Cζ-Nη2 asym st (43); Nε-Cζ (26)	1605	Nη1-Cζ- Nη2 asym st (60); Nε-Cζ-Nη asym bend (17)
1470 (s)	1474 (sh)	1548	Cδ-bend (71); Cγ-bend (13)	1549	Cδ-bend (79)
1445 (s)	1457 (m)	1531	Cγ-bend (46); Cβ-bend 31); Cδ-bend (18)	1530	Cγ-bend (49); Cβ-bend (34); Cδ-bend (12)
1413 (s)	1413 (m)	1521	Cβ-bend (59); Cγ-bend (37)	1519	Cβ-bend (58); Cγ-bend (39)
1388 (sh)		1445	Cγ-wag (33); Cβ-rock (20); Cδ-rock (18)	1449	Cγ-wag (42); Cδ-rock (21); Cβ-rock (15)
1371 (sh)		1429	Cδ-rock (27); $CtOO^-$ sym st (21); Cβ-rock (11); Nt-Cα-Hα (9)	1422	Cδ-rock (22); Cβ-rock (20); $CtOO^-$ sym st (19); Nt-Cα-Hα (9)
1343 (sh)	1343 (w)	1400	$CtOO^-$ sym st (23); Cβ-rock (17); Cδ-rock (11); Cγ-wag (9)	1393	$CtOO^-$ sym st (26); Cδ-rock (12); Cβ-rock (11); Cγ-wag (10)
1331 (s)	1330 (w)	1380	Nt-Cα-Hα (37); Hα-Cα-Cβ (22); Cγ-wag (12); Cδ-rock (9)	1376	Nt-Cα-Hα (31); Hα-Cα-Cβ (25); Cγ-wag (10); Cβ-twist (9); Cδ-rock (9)
1318 (sh)		1367	Cβ-twist (32); Cγ-rock (31); $CtOO^-$ sym st (10)	1366	Cγ-rock (46); Cβ-twist (22)
1296 (m)		1351	Cγ-rock (29); Cδ-twist (22); Ct-Cα-Hα (10)	1348	Cγ-rock (21); Ct-Cα-Hα (17); Cδ-twist (14); $CtOO^-$ sym st (11)
1288 (sh)		1335	Nη2-D_2 bend (19); Nη1-D_2 bend (12); Nη1-Cζ-Nη2 sym st (9); CζNη2D_2 sym bend (9)	1327	Nη2-D_2 (20); Nη1-D_2 (11); Cβ-rock (11); Nη1-Cζ - Nη2 sym st (9)
1251 (w)		1315	Cδ-twist (21); Cβ-rock (16); Cγ-wag (11)	1309	Cβ-rock (22); Cγ-wag (15); Cδ-twist (14)
1215 (w)		1305	Cβ-rock (18); Cγ-wag (18); Cδ-twist (16)	1302	Cδ-twist (27); Cβ-rock (9)
1196 (w)		1255	NtD_3^+ asym bend (18); NtD_3^+ sym bend (14); NtD_3^+ sym rock (13); D$-$O$-$D (W2) (16)	1259	NtD_3^+ asym bend (36); D$-$O$-$D (W3) (9)
1180 (w)	1175 (w)	1239	NtD_3^+ asym bend (25); NtD_3^+ sym bend (20); NtD_3^+ sym rock (18)	1240	NtD_3^+ asym bend (24); NtD_3^+ sym bend (22); NtD_3^+ sym rock (20)
1155 (m)		1223	D-O$-$D (W3) (29); Cβ-twist (10); Cδ-wag (9)	1217	Cβ-twist (21); Cδ-wag (18); Cδ-twist (15); Cγ-rock (9)
1122 (w)		1202	Cδ-Nε (15); Nη2-D_2 bend (14)	1180	Nη2-D_2 (32); CζNη2D_2 sym bend (15); Cδ-Nε (10)
1095 (sh)		1149	Cα-Cβ (16); Cγ-twist (14); Cβ-wag (10); Cδ-wag (9)	1150	Cα-Cβ (17); Cγ-twist (13); Cδ-wag (10); Cβ-wag (9)
		1125	Cγ-Cδ (10)	1124	Cγ-Cδ (9); Ct-Cα-Hα (9)
1084 (m)		1071	Cβ-Cγ (40); Cα-Cβ (17)	1078	Cβ-Cγ (57); Cγ-Cδ (20)
1063 (m)		1068	Cγ-Cδ (39); Cβ-Cγ (14); Cα-Cβ (9)	1070	Cα-Cβ (23)
1025 (w)		1026	Cδ-Nε (25); Cδ-Nε-Hε (11); Nt-Cα (10); W6	1048	Cγ-Cδ (22); Cδ-Nε (15); W6
983 (sh)		997	Nt-Cα (22); Cγ-Cδ (14); Cβ-Cγ (10)	995	Nt-Cα (30)
948 (sh)		972	NtD_3^+ asym rock (18); Nt-Cα (11); Cδ-wag (10)	969	NtD_3^+ asym rock (16); Cδ-wag (11)
907 (s)		935	Nη1-Cζ-Nη2 asym st (27); CζNη1D_2 asym bend (18); Nη1-Cζ-Nη2 sym st (10); W7	955	CζNη1D_2 asym bend (25); Nε-Cζ (10);
		929	Nη1-Cζ-Nη2 (26); Nε-Cζ (15); W10	933	Nη1-Cζ-Nη2 sym st (36); CζNη2D_2 asym bend (11) W6; W8
835 (sh)		886	CζNη1D_2 asym bend (38); CζNη2D_2 asym bend (20); W9	898	CζNη2D_2 asym bend (28); CζNη1D_2 asym bend (19); Cl^-
		879	Cβ-wag (23); Cδ-wag (20); NtD_3^+ asym rock (10)	877	Cβ-wag (24); Cδ-wag (18); NtD_3^+ asym rock (13)
814 (s)		869	NtD_3^+ asym rock (44); Cα-Cβ (11)	865	NtD_3^+ asym rock (47); Cα-Cβ (12); W2
		840	OCtO (21); NtD_3^+ asym rock (13); CαCtOO^- sym bend (11)	833	OCtO (22); NtH3 asym rock (13); CαCtOO^- sym bend (10)
784 (sh)		788	Cβ-Cα-Ct (19); Cγ-twist (16); τ(Cγ-Cδ) (14); τ(Nt-Cα) (12)	785	Cβ-Cα-Ct (19); Cγ-twist(17); τ(Nt-Cα) (14); τ(Cγ-Cδ) (12); W3
738 (w)		764	Cβ-wag (31); Cγ-twist (29); τ(Nt-Cα) 17); Cβ-Cα-Ct (10)	758	Cγ-twist (29); Cβ-wag (28); t(Nt-Cα) (14); t(Cβ-Cγ) (10)
723 (w)		707	ω(Nη1-D_2) (41); ω(Nη2-D_2) (40)	741	ω(Nη2-D_2) (32); ω(Nη1-D_2) (30)

[a] s, intense; m, medium; w, weak; sh, shoulder. Raman: Raman spectra recorded in H_2O buffers (Figure 3). IR: FT-IR ATR spectra recorded in H_2O (Figure 3). Calcd: Calculated wavenumbers obtained at the DFT/B3LYP/6-31++G* the level. See also Figure 5 for optimized geometries. Assignments based on the Potential Energy Distribution (PED). Only major contributions (PED ≥ 9%) are reported. For atom numbering see Figure 1. ω and τ designate an out-of-plane bending and a torsional internal coordinate, respectively. For atom numbering see Figure 1. Water molecules are numbered from W1 to W10 (Figure 5).

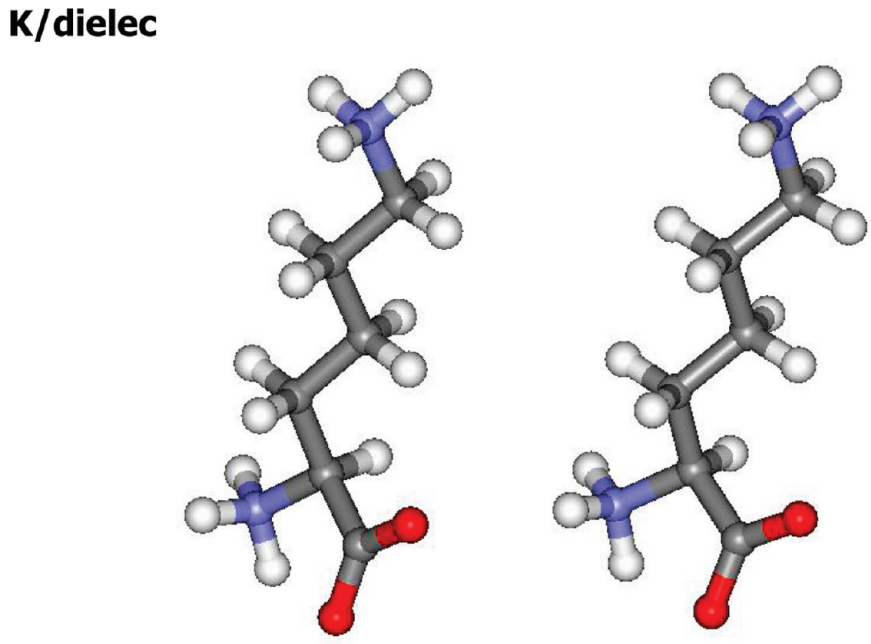

Figure 4. Stereoviews of the geometry optimized lysine (K) placed in a polarizable dielectric continuum mimicking a bulk water environment. See also Table 5 for energy values and Table S1 (Supporting Information) for geometrical parameters.

TABLE 5: Electronic and Vibrational Energies of Hydrated Amino Acids[a]

	polarizable dielectric continuum		
	K/dielec		
E_e	−497.540773		
E_v	141.341		
	explicit hydration		
	$K/8H_2O$ (I)	$K/8H_2O$ (II)	$R/10H_2O$
E_e	−1108.982436	−1108.992147	−1371.386830
E_v	267.730	269.75	304.34
Δ(I−II)	+4.08		
	explicit hydration in the presence of a Cl^- anion		
	$K/8H_2O/Cl^-$ (I)	$K/8H_2O/Cl^-$ (II)	$R/10H_2O/Cl^-$
E_e	−1569.408081	−1569.404344	−1831.815227
E_v	269.873	270.210	305.656
Δ(I−II)	−2.68		

[a] Calculations were performed at the DFT/B3LYP/6-31++G* level of theory. K/dielec: A lysine embedded in a polarizable dielectric continuum. See Figure 4 for the optimized geometry and Table S1 (Supporting Information) for geometrical parameters. $K/8H_2O$: Positively charged cluster formed by a lysine surrounded by 8 water molecules. See Figure 6 for optimized geometries (I and II) and Table S1 (Supporting Information) for geometrical parameters. $K/8H_2O/Cl^-$: Neutral system formed by lysine surrounded by 8 water molecules and a Cl^- anion. See also Figure 6 for optimized geometries I and II. $R/10H_2O$: Positively charged cluster formed by a lysine surrounded by 8 water molecules. See Figure 5 for optimized geometry and Table S2 (Supporting Information) for geometrical parameters. $R/10H_2O/Cl^-$: Neutral cluster formed by an arginine surrounded by 10 water molecules and a Cl^- anion. See Figure 5 for optimized geometry and Table S2 (Supporting Information) for geometrical parameters. E_e: Electronic energy (Hartree). E_v: Zero-point vibrational energy (kcal/mol). Δ (kcal/mol): difference between total energies ($E_{tot} = E_e + E_v$) calculated for the clusters (I) and (II) of lysine, see Figure 6.

IV. Discussion

Effect of Hydration and Cl^- Anion on Geometrical and Energetic Features. The geometric features of lysine embedded in a polarizable dielectric continuum (K/dielec) are taken as reference in our discussion. In this environment, the lysine side chain prefers an *all-trans* conformation, as confirmed by ∼180° values of the three torsion angles defined around the three successive side chain bonds Cβ−Cγ, Cγ−Cδ, and Cδ−Nζ (Table S1, Supporting Information). This extended conformation of the K side chain, corresponding to its lowest-energy orientation, is certainly correlated with the isotopic electric properties of the polarized continuum. In contrast, when lysine is bound to explicit water molecules ($K/8H_2O$), the situation becomes different, and the torsion angle around Cβ−Cγ undergoes a drastic reorientation to *-gauche* region (Table S1, Supporting Information). Due to this conformational change, the lysine side chain is bent, and its terminal $N\zeta H_3^+$ gets closer to the negatively charged group $CtOO^-$ of the backbone (Figures 4 and 6). In the course of geometry optimization on the $K/8H_2O$ cluster, we have found two different low-energy configurations, referred to as (I) and (II) (Figure 6). The main difference between these two configurations is related to the location of the water molecules along the K side chain. For instance, in the $K/8H_2O$ (II), each of the $CtOO^-$ oxygens are H-bonded to two surrounding H_2O (Figure 6). Consequently, the configuration (II) is more stable by 4.08 kcal/mol than its sister configuration (I) (Table 5). We have analyzed the energetic and geometrical changes produced in both of these configurations, in the presence of a Cl^- anion in the vicinity of the side chain terminal $N_\zeta H_3^+$ group (Tables S1, Supporting Information). The neutral cluster $K/8H_2O/Cl^-$ was geometry optimized in both configurations (I) and (II). The presence of Cl^- leads to a substantial rearragement of water molecules around the K side chain terminal $N_\zeta H_3^+$ group (Figure 6). More surprisingly, in the presence of the anion, the energy order of the configurations (I) and (II) is reversed; i.e., the configuration (I) becomes more stable than the configuration (II) by 2.68 kcal/mol (Table 5). It is also to be emphasized that the explicit presence of solvent and counterion around lysine leads not only to perceptible

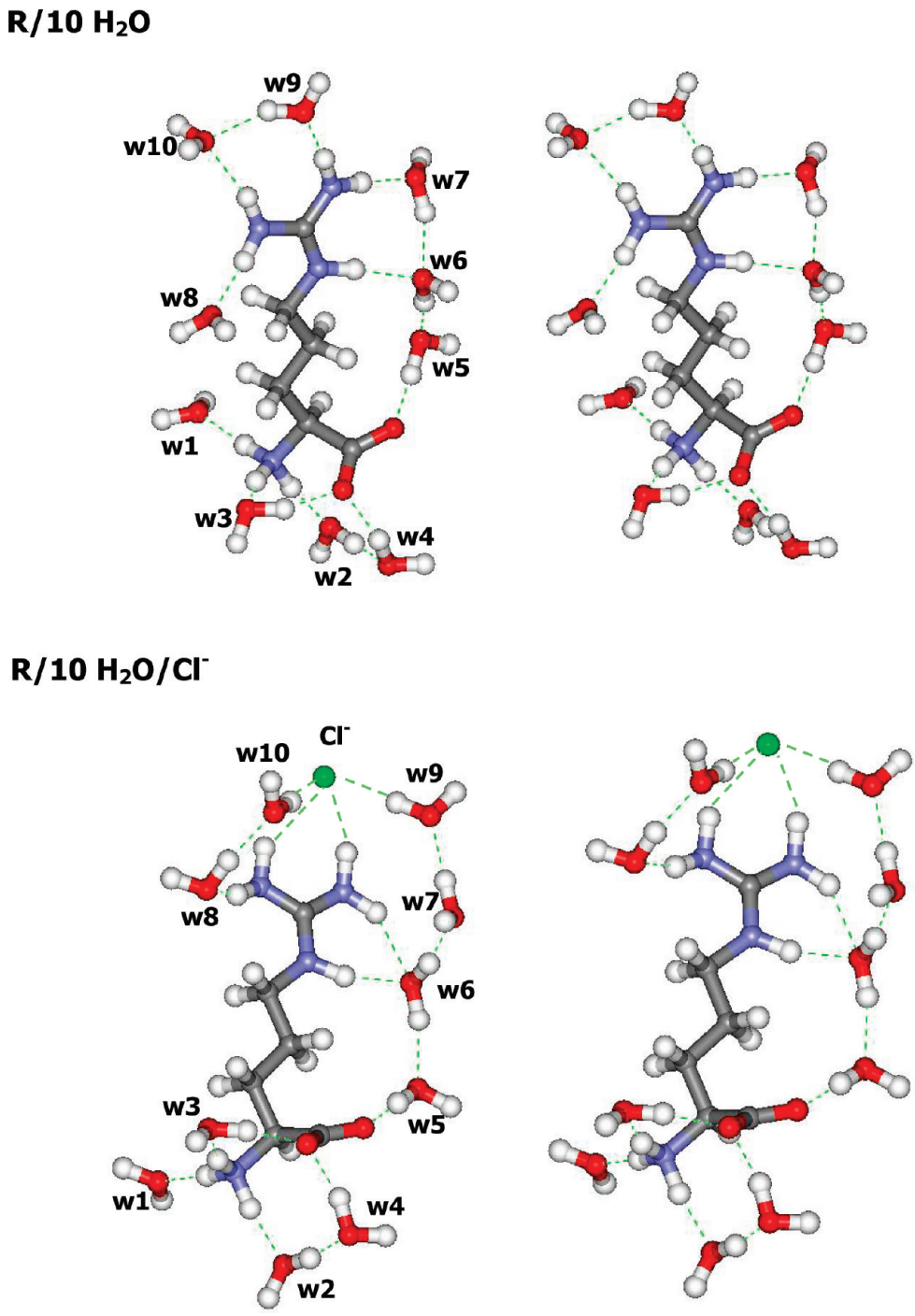

Figure 5. Stereoviews of the geometry optimized arginine (R) in an explicitly hydrated environment. Positively charged cluster R/10H_2O (top). Neutral cluster R/10H_2O/Cl^- (bottom). See Table 5 for energy values and Table S2 (Supporting Information) for geometrical parameters.

changes in the bond lengths and valence angles of the terminal groups but also to other geometrical parameters (Table S2, Supporting Information).

The explicit hydration of arginine does not lead to the same torsion angle behavior as observed in lysine (see above); i.e., the arginine side chain keeps an overall *all-trans* orientation (Table S2, Supporting Information). This can be explained by the presence of the $N_\varepsilon H_\varepsilon$ bond (existent in R and not in K) which stabilizes this conformation through an extra H-bond with one of the surrounding water molecules (Figure 5). However, as in the case of K (see above), the presence of Cl^- leads to a substantial rearrangement of the H-bond network around the R side chain (Figure 5). The bond lengths of all three C−N bonds including the C_ζ atom are included in the 3.33−3.50 Å range (Table S2, Supporting Information). In contrast, the adjacent C_δ−N_ε bond is longer by ∼1 Å compared to the above-mentioned CN bonds (Table S2, Supporting Information). Furthermore, in the absence or presence of the anion, the four atoms C_ζ, N_ε, $N_{\eta 1}$, and $N_{\eta 2}$ remain in the same plane. All these facts prove an equivalent electron delocalization over the $C_\zeta N_\varepsilon$, $C_\zeta N_{\eta 1}$, and $C_\zeta N_{\eta 2}$, bonds. Consequently, none of these bonds manifest a privileged double bond character. Finally, in the positively charged cluster (R/10H_2O) as well as in the neutral cluster (R/10H_2O/Cl^-), the NH_2 groups centered on $\eta 1$ and $\eta 2$ sites of the guanidium group are slightly nonplanar. NH_2 pyramidalization is more important in R/10H_2O compared

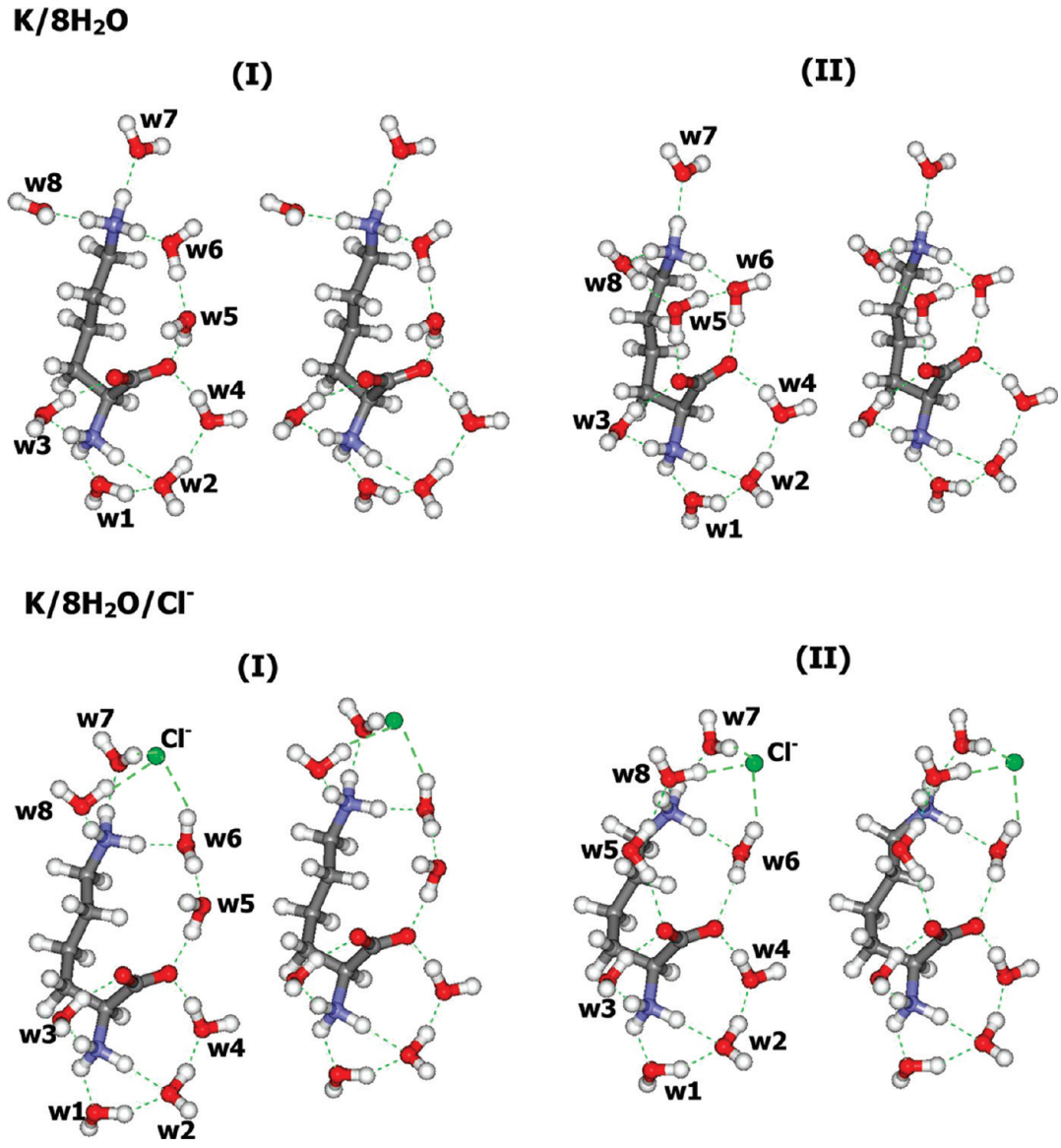

Figure 6. Stereoviews of the geometry optimized lysine (K) in an explicitly hydrated environment. Positively charged K/8H_2O cluster (top). Neutral K/8H_2O/Cl^- cluster (bottom). (I) and (II) refer to two configurations which differ mainly by the H-bond network of the AA with surrounding water molecules. See Table 5 for energy values and Table S1 (Supporting Information) for geometrical parameters.

to that corresponding to R/10H_2O/Cl^-, reflecting the fact that the H-bond network around the R side chain (vide supra) affects differently the nonplanar distortion of its terminal amino groups.

Effect of Hydration and Anion on a Selection of Characteristic Vibrational Modes. To open the discussion on the influence of hydration and anion on the vibrational modes, we have first only reported in Table 6 the characteristic vibrations in which the NH and CO bonds of their terminal groups of the AAs are involved. The most striking effects are observed for NH_3^+ (NtH_3^+ in both AAs and $N_\zeta H_3^+$ in K) angular bendings whose wavenumbers show an upshift of more than 100 cm^{-1} in going from implicit to explicit hydration. The $N_\zeta H_3^+$ in K as well as $N_{\eta 1}H_2$ and $N_{\eta 2}H2$ stretching modes are the most affected by the presence of the anion. One can easily find the correlation between the variation of geometrical parameters (bond lengths and valence angles, see Tables S1 and S2, Supporting Information, for more details) and that of the vibrational wavenumbers upon interaction with explicit water and counterion in K and R. In conclusion, the explicit hydration principally, and the presence of Cl^- to a lesser extent, leads to a global improvement of the above-mentioned characteristic vibrational modes; i.e., their wavenumbers get closer to the spectral ranges where they are generally observed.

Estimation of the Effect of Hydration and Cl^- Anion on the Observed Vibrational Modes in Aqueous Solutions. ***Arginine.*** In Tables 3 and 4 are compared the theoretical wavenumbers obtained from the positively charged (R/10H_2O) and neutral (R/10H_2O/Cl^-) clusters with those observed in Raman and FT-IR spectra of arginine in aqueous solutions (Figure 3). The guanidium group vibrational modes contribute to the complexe and partially resolved bands observed in the 1700−1550 cm^{-1} region. Upon deuteration, the shape of these bands is simplified because of the sensitivity of the corresponding vibrational modes to deuteration. Note the intense FT-IR bands at 1520 cm^{-1}, as well as the intense Raman band at 1092 cm^{-1}, which vanish upon deuteration because both of them originate from the guanidium group vibrational modes. The deuterated counterpart of the Raman mode at 1092 cm^{-1} is the intense mode at 907 cm^{-1} appearing in the D_2O Raman spectrum (Figure 3). Other

TABLE 6: Effect of Implicit and Explicit Hydrations and Counterion on a Selection of Calculated Vibrational Modes[a]

K/continuum	K/8H_2O (I)	K/8H_2O (II)	K/8H_2O/Cl^- (I)	K/8H_2O/Cl^- (II)	R/10H_2O	R/10H_2O/Cl^-	tentative assignments
3350; 3337	3339; 3306	3324; 3285	3369; 3308	3361; 3317	3341; 3044	3376; 3175	NtH_3^+ asymmetric stretch
3280	3112	3124	3100	3103	3160	3084	NtH_3^+ symmetric stretch
1652; 1603	1768; 1761	1746; 1712	1751; 1712	1750; 1722	1770; 1762	1766; 1763	NtH_3^+ asymmetric bending
1488	1620	1622	1616	1619	1639	1635	NtH_3^+ symmetric bending
3322; 3319	3325; 2963	3319; 3045	3152; 2811	3249; 2956			$N\zeta H_3^+$ asymmetric stretcing
3264	3290	3180	3165	3210			$N\zeta H_3^+$ symmetric stretching
1642; 1639	1747; 1704	1782; 1753	1777; 1763	1769; 1753			$N\zeta H_3^+$ asymmetric bending
1521	1645	1636	1685	1665			$N\zeta H_3^+$ symmetric bending
					3606	3500	$N\eta 1H_2$ asymmetric stretching
					3497	3379	$N\eta 1H_2$ symmetric stretching
					1733	1757	H−Nη1-H bending
					3466	3593	$N\eta 2H_2$ asymmetric stretching
					3325	3406	$N\eta 2H_2$ symmetric stretching
					1756	1681	H−Nη2−H bending
					3418	3199	Nε-Hε stretching
1631	1641	1631	1655	1645	1654	1662	C_tOO^- asymmetric stretching
1350	1363	1362	1360	1364	1399	1393	C_tOO^- symmetric stretching

[a] Calculations were performed at the DFT/B3LYP/6-31++G* level of theory. K/dielec: Lysine embedded in a polarizable dielectric continuum. See Figure 4 for optimized geometry and Table S1 (Supporting Information) for geometrical parameters. K/8H_2O: Positively charged cluster formed by a lysine surrounded by 8 water molecules. See Figure 6 for optimized geometry and Table S1 (Supporting Information) for geometrical parameters. K/8H_2O/Cl^-: Neutral system formed by lysine surrounded by 8 water molecules and a Cl^- anion (Figure 6). R/10H_2O: Positively charged cluster formed by a lysine surrounded by 8 water molecules. See Figure 5 for optimized geometry and Table S2 (Supporting Information) for geometrical parameters. R/10H_2O/Cl^-: Neutral cluster formed by an arginine surrounded by 10 water molecule and a Cl^- anion. See Figure 5 for optimized geometry and Table S2 (Supporting Information) for geometrical parameters.

vibrational modes arising from the aliphatic part of the side chain are included in the 1500−1400 cm^{-1} (less sensitive to deuteration) and 1350−1300 cm^{-1} (more sensitive to deuteration) spectral regions.

By the examination of the calculated wavenumbers derived from the R/10H_2O and R/10H_2O/Cl^- clusters, we can confirm that the presence of the anion improves in many cases the agreement between the calculated and observed wavenumbers. In addition, the use of the positively charged cluster (R/10H_2O) alone is not sufficient for assigning the whole vibrational modes observed in aqueous solutions of arginine.

Lysine. Taking into account the discussion on the vibrational modes of arginine (vide supra), we have only reported in Tables 1 and 2 the calculated wavenumbers obtained from the neutral clusters K/8H_2O/Cl^-. Despite their energy difference, both configurations (I) and (II) provide globally similar results, except in the spectral regions corresponding to the $N_\zeta H_3^+$ group and the $CtOO^-$ groups. Upon deuteration, the NtH_3^+ and $N_\zeta H_3^+$ asymmetric bendings, appearing in the 1700−1600 cm^{-1} spectral region, are shifted to lower wavenumber regions. Only a unique and intense band at ∼1615 cm^{-1} remains in this region, mainly arising from the $CtOO^-$ asymmetric bond stretch (Figure 2). In the same manner, the intense IR band at 1523 cm^{-1}, assigned to NtH_3^+ symmetric bending motions, disappers in D_2O (Figure 2). Like in R, the modes involving the aliphatic part of the K side chain give rise to an intense band, nonsenstive to deuteration, in the 1500−1400 cm^{-1} spectral region (Figure 2). In contrast, because of the backbone contribution to the vibrational modes observed in the 1350−1300 cm^{-1} region, they show a higher sensitivity to H/D exchange on labile hydrogens (Figure 2, Tables 1 and 2). Lower spectral regions of both Raman and FT-IR spectra provide other useful information especially on the angular bending motions of the backbone and side chain.

V. Concluding Remarks

On the basis of the aqueous phase vibrational spectra of two major cationic AAs and through a few theoretical examples mimicking their aqueous phase environment, we could basically analyze how the whole molecule may suffer subtle geometrical changes in its bond lengths, valence, and torsion angles, upon interactions with explicit water molecules and in the presence of the counterion. Especially, we have seen that the rearrangement of water molecules around the K side chain may be responsible for the transition between its conformations belonging to its local minima, either in the presence or in the absence of the anion.

From the vibrational point of view, the assignments of the observed modes based on the theoretical calculations show that the internal motions of both AAs are closely coupled to the surrounding water motions (see Tables 1−4 for more details). We have also shown how the presence of the anion and its role in modifying the H-bond network between water and AAs can be appreciated through the analysis of vibrational spectra.

It is a matter of fact that only the quantum mechanical calculations in the presence of explicit water and counterions can provide realistic responses to fundamental questions on geometrical and vibrational features of amino acids in aqueous solution. However, the scope of this investigation was not to elucidate the whole conformations adopted by the amino acid side chains. To achieve this goal, future investigations on the dynamic interactions of the amino acids (and peptides) with water and counterions in hydrated media are necessary.

Acknowledgment. The cooperation between the French (GBM) and Belgian (CRMM) laboratories was supported by a PHC *(Partenariat Hubert Curien)-Tournesol France-Belgique*, ref 13982ZL covering the travels and scientific exchanges between the partners during the period 2007−2008. We would also like to thank two French supercomputer centers: IDRIS (Orsay, France) and CINES (Montpellier, France) for the computational facilities on IBM workstation networks.

Supporting Information Available: Tables S1 and S2, reporting the geometrical parameters as well as atomic Cartesian coordinates of all the optimized geometries discussed in this

report. This material is available free of charge via the Internet at http://pubs.acs.org.

References and Notes

(1) Young, V. R. *J. Nutr.* **1994**, *124*, 1517S–1523S.
(2) Imura, K.; Okada, A. *Nutrition* **1998**, *14*, 143–148.
(3) Reeds, P. J. *J. Nutr.* **2000**, *130*, 1835S–1840S.
(4) Schulz, G. E.; Schrimer, R. H. *Principles of Protein Structure*; Cantor, R. H., Ed.; Springer-Verlag: New York, 1990.
(5) Klug, A.; Rhodes, D.; Smith, J.; Finch, J. T.; Thomas, J. O. *Nature* **1980**, *287*, 509–516.
(6) Kornberg, R. D.; Lorch, Y. *Annu. Rev. Cell Biol.* **1992**, *8*, 563–587.
(7) Delange, R. H.; Smith, E. L. *Annu. Rev. Biochem.* **1971**, *40*, 279–314.
(8) Yeoman, L. C.; Olson, M. O. J.; Sugano, N.; Jordan, J. J.; Taylor, C. W.; Starbuck, W. C.; Busch, H. *J. Biol. Chem.* **1972**, *247*, 6018–6023.
(9) Loret, E. P.; Soto del Valle, R. M.; Mansuelle, P.; Sampieri, F.; Rochat, H. *J. Biol. Chem.* **1994**, *269*, 16785–16788.
(10) Andersson, H.; Bakker, E.; von Heijne, G. *J. Biol. Chem.* **1992**, *267*, 1491–1495.
(11) Audoly, R.; Breyer, R. M. *Mol. Pharmacol.* **1997**, *51*, 61–67.
(12) Fujiwara, Y.; Kubo, Y. *J. Gen. Physiol.* **2006**, *127*, 401–419.
(13) Rawlings, N. D.; Barrett, A. J. *Methods Enzymol.* **1994**, *244*, 19–61.
(14) Derossi, D.; Joliot, A. H.; Chassaing, G.; Prochiantz, A. *J. Biol. Chem.* **1994**, *269*, 10444–10450.
(15) Fernánez-Carneado, J.; Kogan, M. J.; Pujals, S.; Giralt, E. *Biopolymers* **2004**, *76*, 196–203.
(16) Heitz, F.; Morris, M. C.; Divita, G *Br. J. Pharmacol.* **2009**, *157*, 195–206.
(17) Boukhalfa-Heniche, F. Z.; Hernández, B.; Gaillard, S.; Coı¨c, Y. M.; Huynh-Dinh, T.; Lecouvey, M.; Seksek, O.; Ghomi, M. *Biopolymers* **2004**, *73*, 727–34.
(18) Tagounits, A.; Briane, D.; Hernández, B.; Coïc, Y. M.; Ghomi, M.; Cao, A. *Int. J. Biomed. Pharm. Sci.* **2007**, *1*, 135–139.
(19) Derbel, N.; Hernández, B.; Pflüger, F.; Liquier, J.; Geinguenaud, F.; Jaïdane, N.; Ben Lakhdar, Z.; Ghomi, M. *J. Phys. Chem. B* **2007**, *111*, 1470–1477.
(20) Hernández, B.; Pflüger, F.; Nsangou, M.; Ghomi, M. *J. Phys. Chem. B* **2009**, *113*, 3169–3178.
(21) Lima, R. J. C.; Freire, P. T. C.; Sasaki, J. M.; Melo, F. E. A.; Mendes Filho, J. *J. Raman Spectrosc.* **2002**, *33*, 625–630.
(22) Petrosyan, A. M.; Sukiasyan, R. P. *J. Mol. Struct.* **2008**, *874*, 51–56.
(23) Wolpert, M.; Hellwig, P. *Spectrochim. Acta A* **2006**, *64*, 987–1001.
(24) Overman, S. A.; Thomas, G. J., Jr. *Biochemistry* **1999**, *38*, 4018–4027.
(25) Skurski, P.; Gutowski, M.; Barrios, R.; Simons, J. *Chem. Phys. Lett.* **2001**, *337*, 143–150.
(26) Kohn, W.; Sham, L. J. *Phys. Rev.* **1965**, *140*, A1133–A1138.
(27) Becke, A. D. *J. Chem. Phys.* **1993**, *98*, 5648–5652.
(28) Lee, C.; Yang, W.; Parr, R. G. *Phys. Rev B* **1988**, *37*, 785–789.
(29) Frisch, M. J. ; Trucks, G. W.; Schlegel, H. B.; Scuseria, G. E.; Robb, M. A.; Cheeseman, J. R.; Montgomery Jr., J. A.; Vreven, T.; Kudin, K. N.; Burant, J. C.; Millam, J. M.; Iyengar, S. S.; Tomasi, J.; Barone, V.; Mennucci, B.; Cossi, M.; Scalmani, G.; Rega, N.; Petersson, G. A.; Nakatsuji, H.; Hada, M.; Ehara, M.; Toyota, K.; Fukuda, R.; Hasegawa, J.; Ishida, M.; Nakajima, T.; Honda, Y.; Kitao, O.; Nakai, H.; Klene, M.; Li, X.; Knox, J. E.; Hratchian, H. P.; Cross, J. B.; Bakken, V.; Adamo, C.; Jaramillo, J.; Gomperts, R.; Stratmann, R. E.; Yazyev, O.; Austin, A. J.; Cammi, R.; Pomelli, C.; Ochterski, J. W.; Ayala, P. Y.; Morokuma, K.; Voth, G. A.; Salvador, P.; Dannenberg, J. J.; Zakrzewski, V. G.; Dapprich, S.; Daniels, A. D.; Strain, M. C.; Farkas, O.; Malick, D. K.; Rabuck, A. D.; Raghavachari, K.; Foresman, J. B.; Ortiz, J. V.; Cui, Q.; Baboul, A. G.; Clifford, S.; Cioslowski, J.; Stefanov, B. B.; Liu, G.; Liashenko, A.; Piskorz, P.; Komaromi, I.; Martin, R. L.; Fox, D. J.; Keith, T.; Al-Laham, M. A.; Peng, C. Y.; Nanayakkara, A.; Challacombe, M.; Gill, P. M. W.; Johnson, B.; Chen, W.; Wong, M. W.; Gonzalez, C.; Pople, J. A. *Gaussian 03*, revision C.02; Gaussian, Inc.: Wallingford CT, 2004.
(30) Barone, V.; Cossi, M. *J. Phys. Chem. A* **1998**, *102*, 1995–2001.
(31) Cossi, M.; Rega, G.; Scalmani, G.; Barone, V. *J. Comput. Chem.* **2003**, *24*, 669–681.
(32) Dhaouadi, Z.; Nsangou, M.; Hernández, B.; Pflüger, F.; Liquier, J.; Ghomi, M. *Spectrochim. Acta A* **2009**, *73*, 805–814.

JP909517R